Lifting GIS Maps into Strong Geometric Context for Scene Understanding

Raúl Díaz, Minhaeng Lee, Jochen Schubert, Charless C. Fowlkes
Computer Science Department, University of California, Irvine
{rdiazgar,minhaenl,j.schubert,fowlkes}@uci.edu

Abstract

Contextual information can have a substantial impact on the performance of visual tasks such as semantic segmentation, object detection, and geometric estimation. Data stored in Geographic Information Systems (GIS) offers a rich source of contextual information that has been largely untapped by computer vision. We propose to leverage such information for scene understanding by combining GIS resources with large sets of unorganized photographs using Structure from Motion (SfM) techniques. We present a pipeline to quickly generate strong 3D geometric priors from 2D GIS data using SfM models aligned with minimal user input. Given an image resectioned against this model, we generate robust predictions of depth, surface normals, and semantic labels. Despite the lack of detail in the model, we show that the precision of the predicted geometry is substantially more accurate than other single-image depth estimation methods. We then demonstrate the utility of these contextual constraints for re-scoring pedestrian detections, and use these GIS contextual features alongside object detection score maps to improve a CRF-based semantic segmentation framework, boosting accuracy over baseline models.

1. Introduction

The problems of object detection and estimation of 3D geometry have largely been pursued independently in computer vision. However, there seem to be many good arguments for why these two sub-disciplines should join forces. Accurate recognition and segmentation of objects in a scene should constrain matching of features to hypothesized surfaces, aiding reconstruction. Similarly, geometric information should provide useful features and contextual constraints for object detection and recognition. The use of detailed stereo depth has already proven to be incredibly effective in the world of object detection, particularly for RGB-D sensors in indoor scenes [14, 24]. More general formulations have attempted to jointly integrate geometric reconstruction from multiple images with scene and object recognition [4, 5, 20]. On the other hand, works such as [19, 13, 30, 37] have focused on the role of context in a single image, operating under the assumption that the camera and scene geometry are unknown and must largely be inferred based on analysis of monocular cues. This problem is quite difficult in general although some progress has been made [18, 34, 8], particularly on indoor scenes of buildings where the geometry is highly regular [33, 15, 16].

In this paper, we argue that a huge number of photographs taken in outdoor urban areas are pictures of known scenes for which rich geometric scene data exists in the form of GIS maps and other geospatial data resources. Robust image matching techniques make it feasible to resection a novel image against large image datasets to produce estimates of camera pose on a world-wide scale [23]. Once a test photo has been precisely localized, much of this contextual information can be easily backprojected into the image coordinates to provide much stronger priors for interpreting image contents. For the monocular scene-understanding purist, this may sound like "cheating", but from an applications perspective, such strong context is already widely available or actively being assembled and should prove hugely valuable for improving the accuracy of image understanding.

To study the role of strong geometric context for image understanding, we have collected a new dataset consisting of over six thousand images covering a portion of the UC Irvine campus for which relative camera pose and 3D coordinates of matching points has been recovered using structure from motion. We describe a method for aligning this geometric and photometric data with 2D GIS maps order to quickly build 3D polygonal models of buildings, sidewalks, streets and other static structures with minimal user input (Section 3). This combined geosemantic context dataset serves as a reference against which novel test images can be resectioned, providing a rich variety of geometric and semantic cues for further image analysis. We develop a set of features for use in detection and segmentation (Sections 4 and 5) and experimentally demonstrate that these contextual cues offer significantly improved performance with respect

This work was supported by NSF IIS-1253538 and a Balsells Fellowship to RD.

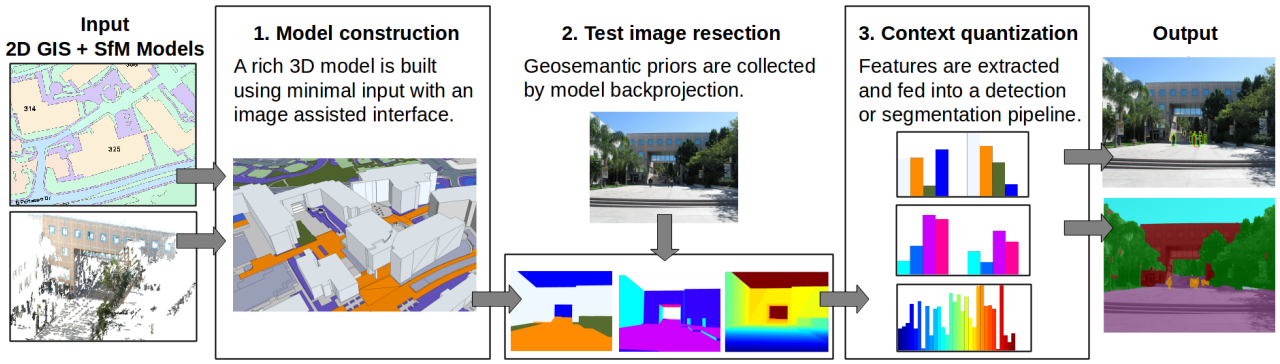

Figure 1: System overview: 2D GIS and SfM data are aligned to build a 3D model with minimal effort using an image-assisted Sketchup plug-in. This fused geocontext provides a basis for efficiently transferring rich geometric and semantic information to a novel test image where it is used to improve performance of general scene understanding (depth, detection, and segmentation).

to strong baselines for scene depth estimation, pedestrian detection and semantic segmentation (Section 6).

2. Contribution and Related Work

The contribution of our work is twofold. First, we demonstrate a pipeline that performs precise resectioning of test images against GIS map data to generate geosemantic context applicable to multiple scene understanding tasks. Secondly, we show that simple cues derived from the GIS model can provide significantly improved performance over baselines for depth estimation, pedestrian detection and semantic segmentation. We briefly discuss the differences between our results and closely related work. Figure 1 shows an overview of the system pipeline.

GIS for image understanding The role of GIS map data in automatically interpreting images of outdoor scenes appears to have received relatively little attention in computer vision. While detailed GIS map data is used extensively in analysis of aerial images [38, 39, 32], only a handful of papers have exploited this resource to study scene understanding from a ground-level perspective. Recently, a few groups have looked at using GIS data and multi-view geometry for improving object recognition. [27] introduced a geographic context re-scoring scheme for car detection based on street maps. Ardeshir et al. used GIS data as a prior for static object detection and camera localization [3] and for performing segmentation of street scenes [2]. Compared to these works, our pipeline utilizes full 6D camera pose estimation and a richer scene model derived from the GIS map that supports not only improved detection rescoring but also depth and semantic label priors.

Perhaps most closely related work to our approach is [40] which uses a CRF to simultaneously estimate depth and scene labels using a strong 3D model. However, [40] assumes that both camera localization and a CAD model of a scene with relevant categories (e.g., trees) are provided as inputs. In contrast, we address the construction of a 3D scene model by combining image and map data as well as test-time camera localization using model alignment and resectioning techniques. Interestingly, we also show that lifted GIS data can improve segmentation accuracy even for semantic labels that are not present in the GIS map model (e.g., trees, retaining walls).

Contextual detection rescoring Rescoring object detector outputs based on contextual and geometric scene constraints has been suggested in a wide variety of settings. For example, Hoiem et al. [17] used monocular estimation of a ground-plane to rescore car and pedestrian detections, improving the performance of a contemporary baseline detector [6]. Similarily, [3] showed improvement on hard to detect objects such as fire hydrants. However, the benefit of scene geometry constraints appears to be substantially less when a more robust baseline detector such as DPM [9] is used. For example, [7] reported that monocular ground-plane constraints failed to improve the performance of a DPM pedestrian detector. Similarly, [27] reported that geometric rescoring based on road maps did not improve performance of a DPM car detector (although rescoring did improve detection for a weaker detector that had been trained to predict viewpoints). In contrast to this previous work, we use a richer rescoring model that allows for non-flat supporting surfaces and integrates additional geosemantic cues, resulting in a significant boost (5% AP) in pedestrian detection even when rescoring a strong baseline model.

3. Lifting GIS Maps

In this section, we describe the construction of a dataset for exploring the use of strong GIS-derived geometric context. We focus on novel aspects of this pipeline which include: aligning GIS and SfM data, a user-friendly toolbox to lift 2D geosemantic information provided by a map into 3D geometric context models, and model-assisted camera

resectioning to allow quick and accurate localization of a test image with respect to the context model.

Image database acquisition We collected a database of 6402 images covering a large area (the engineering quad) of UC Irvine's campus. Images were collected in a systematic manner using a pair of point and shoot cameras attached to a monopod. We chose locations so as to provide approximately uniform coverage of the area of interest. Images were generally collected during break periods when there were relatively few people present (although some images still contain pedestrians and other non-rigid objects). The dataset is available at http://vision.ics.uci.edu/datasets/.

Running off-the-shelf incremental structure from motion (e.g., [1, 36]) on the entire dataset produces a 3D structure that is qualitatively satisfying but often contains metric inaccuracies. In particular, there can be a significant drift over the whole extent of the recovered model that makes it impossible to globally align the model with GIS map data. These reconstruction results were highly dependent on the quality of the initial matches between individual camera pairs. However, we found that the excellent incremental SfM pipeline implementation in OpenMVG [29], which uses the adaptive thresholding method of [28], yielded superior results in terms of the accuracy and number of recovered cameras and points. Our final model included 4929 succesfully bundled images.

Global GIS-structure alignment We obtained a 2D GIS map of the campus maintained by the university's building management office. The map was originally constructed from aerial imagery and indicates polygonal regions corresponding to essential campus infrastructure tagged with semantic labels including building footprints, roadways, firelanes, lawns, etc.

We would like to align our SfM reconstruction with this model. One approach is to leverage existing sets of geo-referenced images. For example, [27] used aerial LiDAR and Google Street View images with known geocoordinates in order to provide an absolute coordinate reference. While this is practical when the 3D GIS data has already been generated, we start from a flat 2D model depicting an environment for which no precisely georegistered images were readily available.

To quickly produce an initial rough alignment, we project the point cloud recovered using SfM onto a ground-plane and have a user select 3 or more points (typically building corners as they are more visible). We run Procrustes alignment to match the user selected points to the real coordinates in our 2D GIS data. This global 2D alignment is sufficient to register the SfM model in geographic coordinates for the intial construction of a 3D model. Once the 3D GIS model is defined (see below), we used an iterative closest point approach to automatically refine the alignment of the GIS model and SfM point cloud.

Figure 2: We developed a custom Sketchup plug-in that imports camera parameters computed during bundle adjustment. The user easily models the 3D geometry by extruding, tilting, and carving the 2D map data until it naturally aligns with the image.

Image-assisted 3D model construction We developed a custom plug-in for the 3D modeling tool Sketchup to allow efficient user-assisted "lifting" of 2D GIS map data into a full 3D model. We imported the GIS 2D polygons with their corresponding semantic labels into the workspace. The user is then presented with a choice of images to load from the globally aligned SfM model. When an image is selected, the 3D model view is adjusted to match the recovered camera extrinsic and intrinsic parameters and the image is transparently overlayed, providing an intuitive visualization as shown in Figure 2. The user can then extrude flat 2D polygons (e.g., building footprints) to the appropriate height so that the backprojected view into the selected camera matches well with the overlayed image.

A full 3D mesh model can be easily constructed starting from the aligned 2D map by extruding buildings up, carving stairs down, tilting non-fully horizontal surfaces, etc. using standard Sketchup modeling tools and guided by the image overlay. Additional geometry can be easily created, as well as adding additional semantic labels or corrections to the original data. With the assistance of these aligned camera views, constructing a fairly detailed model in Sketchup covering 10 buildings took approximately 1-2 hours. This can be considered an offline task since the modeling effort is performed only once, as buildings are largely static over time.

GIS-assisted test image resectioning To estimate camera pose at test time, we resection each test image against the SfM image dataset based on 2D-3D matching correspondences using a RANSAC-based 3-point absolute pose procedure [21]. We developed several techniques for improving the accuracy of this resectioning. As the bundled image dataset grows to cover larger areas, resectioning accuracy generally falls since the best match for a given feature descriptor in the test image is increasingly likely to be a false positive. To leverage knowledge of spatial locality and scale to large datasets, we partitioned the bundled cameras into $k = 10$ clusters using k-means over database camera positions. Points in the bundled model were included in

any camera cluster in which they were visible yielding 10 non-disjoint clusters of points.

Each test image was resectioned independently against each spatial cluster and the best camera pose estimate among the clusters was selected using geometric heuristics based on the GIS model. We measured the distance to ground (height) and camera orientation with respect to the gravity direction in the GIS model. All camera poses below the ground plane, higher than 4 meters, or tilted more than 30 degrees were discarded. If a camera pose was geometrically reasonable in more than one cluster, we selected the estimate with the highest number of matched inliers. *Incorporating these heuristic constraints increased the proportion of correctly resection test images substantially (from 49% to 59%).* This improvement would not possible without the GIS-derived 3D model since the ground elevation varies significantly and cannot be captured by a simple global threshold on the camera coordinates.

Resectioning of a test image produces immediate predictions of scene depth, surface orientation, and semantic labels at every image pixel. It is interesting to compare these to previous works that attempt to estimate such geometric or semantic information from a single image. By simply resectioning the picture against our 3D model we are immediately able to make surprisingly accurate predictions without running a classifier on a single image patch! In the remainder of the paper, we discuss how to upgrade these "blind" predictions by incorporating backprojected model information into standard detection and segmentation frameworks.

4. Strong Geometric Context for Detection

Estimating camera pose of a test image with respect to a 3D GIS model aids in reasoning about the geometric validity of hypothesized object detections (e.g., pruning false positives in unlikely locations or boosting low-scoring candidates in likely regions). We describe a collection of features that capture these constraints and use them to improve detection performance. We incorporate these features into a pedestrian detector by training an SVM with geometric context features (GC-SVM) that learns to better discriminate object hypotheses based on the geosemantic context of a candidate detection.

3D geometric context Let a candidate 2D bounding box in a test image I have an associated height in pixels h^{im}. We use a deformable part model that consists of a mixture over three different template filters: full-body, half upper body, and head. We set the image detection height h^{im} based on which mixture fires as 1, 2 or 3 times the bounding box height respectively.

If we assume that the object is resting on a horizontal surface and the base of the object is visible, then we can estimate the 3D location the object is occupying. We find the depth at intersection z_i of the object with respect to the camera by shooting a ray from the camera center through the bounding box's "feet" and intersecting it with the 3D model. Importantly, unlike many previous works, the ground is not necessarily a plane (e.g., our model includes ground at different elevations as well as stairs and ramps). Given camera focal length f, we can estimate the height in world coordinates by the following expression:

$$h_i = \frac{z_i}{f} h^{im} \tag{1}$$

Unfortunately, the object's "feet" might not be visible at all times (e.g., a low wall is blocking them). Let h_μ be the "physical height" of an average bounding box (i.e., the height of an average human). We collect all possible intersections with the model (e.g., both the intersections with a blocking wall and the ground plane hehind it) and choose the h_i that minimizes $(h_i - h_\mu)^2$.

An alternative method to hypothesize an object's height is by its inverse relation with depth. We can estimate an object's depth z_o based on the expected average human height h_μ. A bounding box of size h^{im} in the image has an expected distance

$$z_o = h_\mu \frac{f}{h^{im}} \tag{2}$$

from the camera. Given z_o, we produce a second height estimate h_o by tracing a ray through the center top of the detection to a depth z_o and then measuring the distance from this estimated head position to the ground plane.

For each height estimator h_i, h_o we also extract a corresponding semantic label associated with the GIS-model polygon where the feet intersect and record binary variables w_i, w_o indicating whether the polygon has a "walkable" semantic label and n_i, n_o indicating wheter it has a horizontal surface normal. Our feature vectors for each estimate are given by:

$$F_i = [v_i(h_i - h_\mu)^2, w_i, n_i, (1 - v_i)] \tag{3}$$

$$F_o = [v_o(h_o - h_\mu)^2, w_o, n_o, (1 - v_o)] \tag{4}$$

where $h_\mu = 1.7m$ is the average human height and v_i, v_o are binary variables indicating whether the the corresponding height cound be measured. For example, if the ray to the foot to compute z_i does not intersect the model or if the depth estimate z_o is behind the model surface, we mark the estimate as invalid and zero out all but the last entry of the feature vector.

2D geosemantic context In addition to the height and foot location, we extract geosemantic context by backprojecting model semantic labels and surface normals into the image plane and look at the distribution inside of the object bounding box. For each bounding box b, we hypothesize a full-body bounding box given the detection's mix-

ture as previously mentioned. We then split such box vertically into 3 parts (top, center, bottom) and collect normalized histograms H_b of the distribution of semantic labels and surface normals in each subregion. We account for 5 GIS labels (building, plants, pavement, sky, unknown) and 4 discretized surface normal directions (ground, ceiling, wall, none).

$$H_b = [H_{top}, H_{center}, H_{bottom}] \quad (5)$$

To allow the learned SVM weights to depend on the original detector mixture component m, we contruct an expanded feature vector from these histograms:

$$F_b = [\delta(m=1)H_b, \delta(m=2)H_b, \delta(m=3)H_b] \quad (6)$$

where $m \in 1, 2, 3$ indicates a full-body, upper-half, or head mixture respectively. For example, this allows us to model that upper-body detections are correlated with the presence of some vertical, non-walkable surface such as a wall occluding the lower body.

We train an SVM to rescore each detection using a final feature vector that includes the detector score s along with the concatenated context features

$$F = [s, F_i, F_o, F_b]$$

5. Strong Geometric Context for Segmentation

The geometric and semantic information contained in the GIS data and lifted into the 3D GIS model can aid in reasoning about the geometric validity of class hypotheses (e.g., horizontal surfaces visible from the ground are not typically buildings). We describe methods for using such constraints to improve semantic segmentation performance. We follow a standard CRF-based labeling approach from Gould et al. [12] which uses an augmented set of image features from [35]. We explore simple ways to enhance this set of features using GIS data and study its influence on semantic labeling accuracy.

GIS label prior distributions The GIS-derived model provides an immediate estimation of pixel labels based on the 4 semantic labels in the original GIS map (building, plants, pavement, and sky). If a camera pose is known, we can backproject the model into the image plane and transfer the polygon label in the GIS model to the projected pixel. However, camera pose estimation is not perfect and might contain minimal deviations from its ground truth pose. In order to account for slight camera pose inaccuracies, we define a 16-dimensional feature descriptor to softly handle these cases. Given an image I, a pixel $x \in I$, and a backprojected GIS semantic label $g(x)$, we define the feature $h^r_k(x)$

$$h^s_{r,k}(x) = \frac{1}{N} \sum_{y:\|y-x\|<r} \delta(g(y) = k) \quad (7)$$

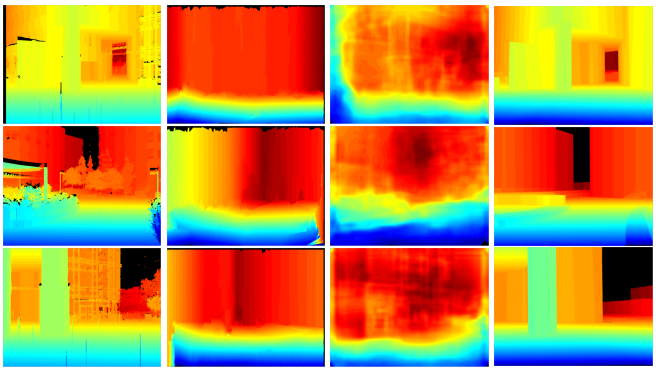

Ground Truth | Make3D [34] | DNN [8] | GIS

Figure 3: Qualitative depth comparison. Our GIS backprojected depth map is shown in the last column. While it lacks many details such as foliage and pedestrians which are not included in our coarse GIS-based 3D model, simply backprojecting depth provides substantially more accurate estimation than existing monocular approaches.

as the normalized count of class k pixels in a circular disc of radius r around x, where N is the number of pixels in the disc. In our experiments, we define r so that the angular error of the camera pose is 0, 1, 3, and 5 degrees.

GIS surface normal distributions In a similar manner, a surface normal can be quickly estimated for any pixel by backprojecting the 3D model into the camera plane. Surface normals can be discriminative of certain classes like pavement, roads, buildings, etc. Following the same structure as in equation 7, we define the 12-dimensional feature $h^r_n(x)$ as

$$h^n_{r,k}(x) = \frac{1}{N} \sum_{y:\|y-x\|<r} \delta(n(y) \in N_k) \quad (8)$$

where N_k is one of 3 possible surface orientation bins: horizontal (ground), horizontal (ceiling), vertical (wall).

GIS Depth features Depth can also be efficiently estimated from a 3D model when a camera pose is known. Following other methods like [42], we extract HOG features [6] to encode depth variations. We did find a substantial gain in certain categories when adding these features into the model (e.g., wall).

DPM as a context feature Inspired by other works that try to create segmentation-aware detectors [10, 22, 26, 31], we also incorporate the outputs of category-specific object detectors in our segmentation model. To do so, we collect the scores of a DPM detector for an object category c and generate a DPM feature map h_c by assigning to every pixel the maximum score of any of the candidate detection boxes intersecting the given pixel. Let Ω_c be the set of candidate detections and b_i, s_i the bounding box and score for the ith

detection, then

$$h_c^o(x) = \max_{i \in \Omega_c}(s_i \cdot \delta(x \in b_i)) \quad (9)$$

6. Experimental results

In our experiments, we started with a test set comprising 570 pictures taken in the area covered by the 3D model. These images were collected over different days and several months after the initial model dataset was acquired. Of these images, 334 images (59%) were successfully resectioned using the cluster-based approach from Section 3. This success rate compares favorably with typical success rates for incremental bundle adjustment (e.g., [27] register 37% of their input images) even though our criteria for correctness is more stringent (we manually scored test images rather than relying on number of matching feature points). To evaluate performance of detection, we annotated resectioned images with ground-truth bounding boxes for 1484 pedestrians using the standard PASCAL VOC labeling practice including tags for truncated and partially occluded cases. We used 167 images for training our geometric context rescoring framework and left the remaining 167 for testing. We also manually segmented 305 of these images using the segmentation tool provided by [25] and labeled each segment with one of 9 different semantic categories. We split the segmentation data into 150 images for training and 155 for testing.

6.1. Monocular Depth Estimation

To verify that the coarse-scale 3D GIS model provides useful geometric information, despite the lack of many detailed scene elements such as trees, we evaluated resectioning and backprojection as an approach for monocular depth estimation. While our approach is not truly monocular since it relies on a database of images to resection the camera, the test time data provided is a single image and constitutes a realistic scenario for monocular depth estimation in well photographed environments.

To establish a gold-standard estimate of scene depth, we scanned 14 locations of the area covered by our dataset using a Trimble GX3D terrestrial laser scanner. We took the scans at in a range of resolution between 5 and 12 cm in order to keep the total scanning time manageable, resulting in roughly a half a million 3D points per scan. We mounted a camera on top of the laser scanner and used the camera focal length to project the laser-based 3D point cloud onto the camera image plane, interpolating depth values to obtain a per-pixel depth estimate. We then resectioned the test image and synthesized the depth map predicted by our 3D GIS model.

Threshold	Make3D	DNN	GIS
$\delta < 1.25$	11.03%	28.21%	67.04%
$\delta < 1.25^2$	30.71%	45.09%	82.37%
$\delta < 1.25^3$	49.47%	56.04%	88.25%

Figure 4: Quantitative comparison of depth estimation methods: Make3D [34], Deep Neural Network [8], and GIS backprojection. We list the proportion of depths within a specified maximum allowed relative error $\delta = \max(\frac{d_{gt}}{d_{est}}, \frac{d_{est}}{d_{gt}})$, where d_{gt} is the ground truth depth and d_{est} is the estimated depth at some point. The DNN model predictions were re-scaled to match our ground truth data since the model provided is adapted only for indoor scenes and it was not practical to collect enough laser scans to retrain the model for our dataset.

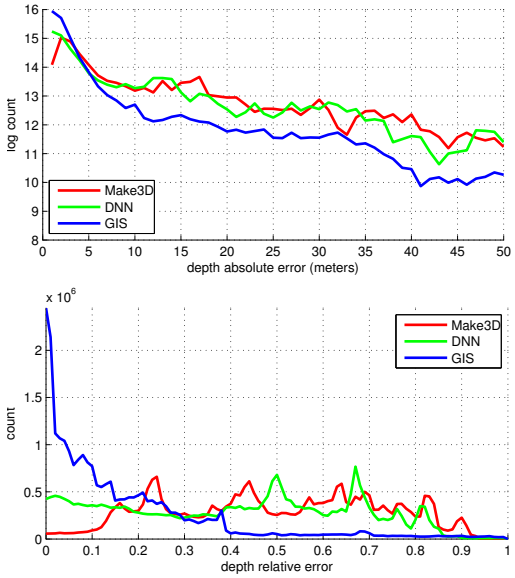

Figure 5: Accuracy of predicted depth estimates compared to gold-standard provided by a laser-scanner for 14 images. Top histogram shows the distribution (log counts) of absolute depth errors between Make3D, DNN and depth computed from resectioning and backprojecting GIS derived 3D model. The bottom plot shows the distribution of relative error $|d_{est} - d_{gt}|/d_{gt}$.

Figure 4 shows quantitative results of our GIS backprojection depth estimation against other single-image depth approaches for the 14 scan dataset. We used the provided pre-trained models included in [34, 8] as baselines for comparison. Since the pretrained DNN model [8] was only available for indoor scenes (trained from Kinect sensor data), we estimated a scaling and offset factors for the output that minimized the relative error over the 14 images. While the scaled pretrained DNN model is probably suboptimal, it is not possible to retrain the model without collecting substantially larger amounts of training data using specialized hardware (a laser scanner). In contrast, our proposed approach of simply backprojecting GIS data greatly outperforms image-predictions using only camera pose and a map, with no training data required!

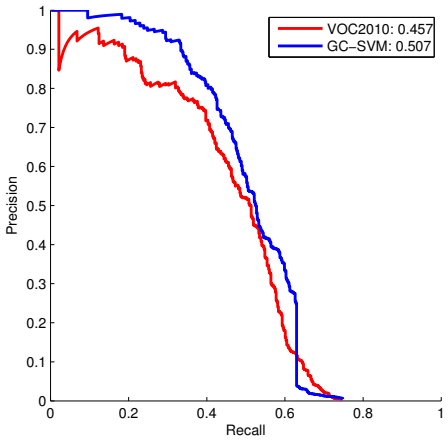

Figure 6: Geometric context aids in recognizing discriminative 3D and 2D features that improve the average precision in pedestrian detection. Our GC-SVM obtained a 5% boost in AP with respect to the standard DPM model.

6.2. Object Detection

We evaluated our geometric and semantic object rescoring scheme applied to the widely used deformable part model detector (DPM) [9]. We used a standard non-maxima suppression ratio of 0.5 in the intersection over union overlap.

Of the 167 training image split, we ran DPM and collected the set of geometric context features F described in Section 4 along with the appropriate label indicating whether the bounding box was a true or false positive. We trained a linear SVM classifier where we set the regularization $C = 4$ using 5-fold cross-validation. To accommodate class imbalance and maximize average precision, we used cross-validation to set the relative penalty for misclassified positives to be $4x$ larger than for negatives.

On test data the standard DPM detector score provided a baseline average precision (AP) of **0.457**, while our GC-SVM model based on geosemantic features F achieved an AP of **0.507**. It is important to note that previous attempts to incorporate GIS-based geometric rescoring into a DPM classifier provided little to no improvement. In [27], 3D context between cars and streets allowed for improved geometric reasoning about car orientation but only small gains in detection performance. In fact their final VP-LSVM and VP-WL-SSVM models had lower average precision than a baseline DPM model.

6.3. Semantic Segmentation

We built two baseline segmentation models using the CRF-based multi-class segmentation code provided by [11]. We trained one model using our labeled training set of engineering quad images (CRF ENGQ) as a scene-specific model. We also trained a generic model using images collected from the SUN dataset [41] by querying for multiple categories in the SUN label set that are semantically equivalent to the 9 categories labeled in our engineering quad dataset (CRF SUN). Finally, we added our GIS and DPM features to the ENGQ model and evaluated their effects on segmentation performance.

DPM GC-SVM

Figure 7: Detection results at 0.6 recall. Geosemantic context successfully removes high score false positives at unlikely places without adding too many low score ones at coherent regions. This successful trade-off benefits the performance at almost all levels of recall.

Detectors Improve Segmentation We collected DPM score features as described previously for two objects of interest: pedestrian and bicycle. Figure 8 shows the influence of adding these features into the model (+DPM rows). We raised pedestrian segmentation accuracy from 0.400 to 0.583 and bicycle from 0.370 to 0.482 in the ENGQ model.

It is interesting to note how these detection priors mix with geosemantic information. In the presence of geometric context, pedestrian segmentation was slightly hurt. However, sitting pedestrian segmentation is boosted from almost 0 accuracy up to 0.108. Bicycle also benefits from geometric context and boosts from 0.458 to 0.530.

GIS-aware Segmentation To evaluate the influence of GIS features alone, we first trained a CRF model without the image features from [12] and only used the contextual features described in Section 5 (GIS CRF). This yielded relatively good accuracy in the 4 labels present in the GIS

Model	Overall	building	plants	pavement	sky	ped.	ped. sit	bicycle	bench	wall
GIS Label Backprojection	0.242	0.688	0.099	0.810	0.581	0.000	0.000	0.000	0.000	0.000
GIS CRF	**0.290**	**0.730**	**0.316**	**0.847**	**0.705**	0.000	0.000	0.000	0.000	**0.014**
Image CRF (ENGQ)	0.561	0.917	0.886	0.925	0.949	0.400	0.010	0.370	0.241	0.348
+GIS	0.584	0.937	0.894	0.936	0.963	0.394	0.060	0.385	0.208	**0.481**
Depth	0.569	0.935	**0.895**	0.937	0.957	0.390	0.011	0.358	0.179	0.455
Labels	0.575	**0.938**	0.892	0.933	**0.966**	0.374	0.064	0.366	0.221	0.419
Normals	0.568	0.935	0.893	0.933	0.961	0.389	0.007	0.385	0.192	0.418
+DPM	0.590	0.920	0.892	0.929	0.947	**0.583**	0.013	0.482	0.184	0.360
+DPM+GIS	**0.627**	0.936	0.894	**0.938**	0.961	0.568	**0.108**	**0.520**	**0.245**	0.472

Figure 8: Quantitative segmentation results for models trained with generic (SUN) and scene specific (ENGQ) data. Accuracy is measured using PASCAL intersection-over-union (IOU) protocol. Adding geosemantic (+GIS) and detection (+DPM) features outperformed the baseline models. Combining both methods gave the best overall results in the scene specific model.

model, but poor results for many others. This is quite natural since our GIS model does not include detailed elements such as benches, and provides no information about what pixels might be a bike or pedestrian on any given day. However, this model still improves a simple "blind" backprojection of the GIS labels.

On the other hand, combining these GIS features with standard image features gave a significant benefit, outperforming the image CRF baseline in almost all categories (+GIS rows in Figure 8). It is interesting to note that labeling of some categories that did not appear in the GIS map data (e.g., bench and wall) is still improved significantly by the geometric context provided in the model (wall is boosted from 0.348 to 0.481, presumably since the local appearance is similar to building but the geometric context is not). This is in contrast to, e.g., [40], where all labels were included in either the GIS or detector driven priors.

Scene Specific vs Generic Models Even without precisely resectioning the test image, there is a significant gain in accuracy from knowing the rough camera location. When the camera location is completely unknown, the best we can do is invoke the CRF trained on generic SUN data (0.309 accuracy). However, if we know the camera is located somewhere on the engineering quad, we can invoke the scene specific CRF trained on ENGQ to boost performance to 0.561. With resectioning, we can further utilize the 3D model (+GIS) to gain an additional 3% in segmentation performance by utilizing geosemantic context features in the unary potential classifier. This gain is quite significant given that some class baselines are already over 90% in accuracy leaving little room for improvement.

7. Conclusion

The rapid growth of digital mapping data in the form of GIS databases offers a rich source of contextual information that should be exploited in practical computer vision systems. We have described a basic pipeline that allows for integration of such data to guide both traditional geometric reconstruction as well as semantic segmentation and recognition. With a small amount of user supervision, we can quickly lift 2D GIS maps into 3D models that immediately provide strong scene geometry estimates (typically less than 5-10% relative depth error), greatly outperforming existing approaches monocular depth estimation and providing a cheap alternative to laser range scanners. This also provides strong geometric and semantic context features that can be exploited to improve detection and segmentation.

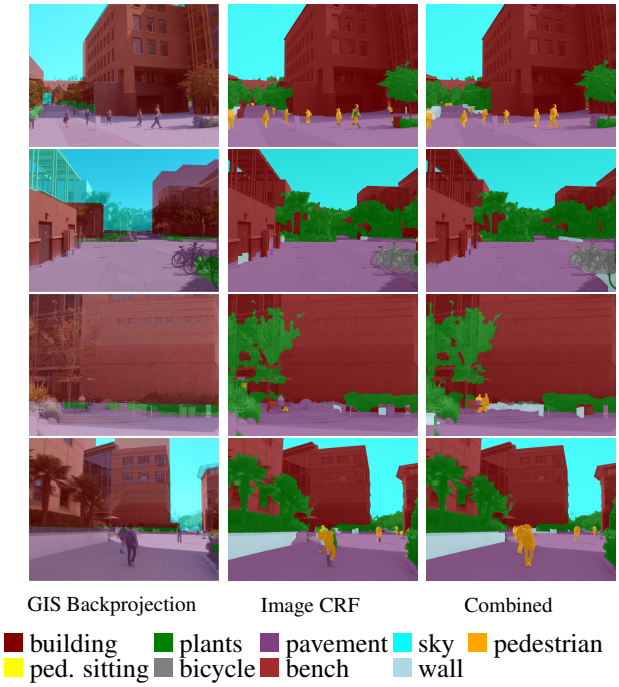

Figure 9: Qualitative segmentation results with overlaid images. Our combined model improves over a image-based CRF by incorporating features derived from GIS (depth, labels, normals) and a DPM detector.

References

[1] S. Agarwal, N. Snavely, I. Simon, S. Seitz, and R. Szeliski. Building rome in a day. *ICCV*, 2009. 3

[2] S. Ardeshir, K. M. Collins-Sibley, and M. Shah. Geo-semantic segmentation. In *CVPR*, 2015. 2

[3] S. Ardeshir, A. R. Zamir, A. Torroella, and M. Shah. Gis-assisted object detection and geospatial localization. In *ECCV*. 2014. 2

[4] S. Y. Bao, M. Bagra, Y.-W. Chao, and S. Savarese. Semantic structure from motion with points, regions, and objects. In *CVPR*, 2012. 1

[5] N. Cornelis, B. Leibe, K. Cornelis, and L. Van Gool. 3d urban scene modeling integrating recognition and reconstruction. *IJCV*, 2008. 1

[6] N. Dalal and B. Triggs. Histograms of oriented gradients for human detection. In *CVPR*, 2005. 2, 5

[7] R. Diaz, S. Hallman, and C. C. Fowlkes. Detecting dynamic objects with multi-view background subtraction. In *ICCV*, 2013. 2

[8] D. Eigen, C. Puhrsch, and R. Fergus. Depth map prediction from a single image using a multi-scale deep network. In *NIPS*, 2014. 1, 5, 6

[9] P. F. Felzenszwalb, R. B. Girshick, D. McAllester, and D. Ramanan. Object detection with discriminatively trained part-based models. *TPAMI*, 2010. 2, 7

[10] S. Fidler, R. Mottaghi, A. Yuille, and R. Urtasun. Bottom-up segmentation for top-down detection. In *CVPR*, 2013. 5

[11] S. Gould. Darwin: A framework for machine learning and computer vision research and development, v1.9. *JMLR*, 2012. 7

[12] S. Gould, R. Fulton, and D. Koller. Decomposing a scene into geometric and semantically consistent regions. In *ICCV*, 2009. 5, 7

[13] A. Gupta, S. Satkin, A. A. Efros, and M. Hebert. From 3d scene geometry to human workspace. In *CVPR*, 2011. 1

[14] S. Gupta, R. Girshick, P. Arbeláez, and J. Malik. Learning rich features from rgb-d images for object detection and segmentation. In *ECCV*. 2014. 1

[15] V. Hedau, D. Hoiem, and D. Forsyth. Recovering the spatial layout of cluttered rooms. In *ICCV*, 2009. 1

[16] V. Hedau, D. Hoiem, and D. Forsyth. Thinking inside the box: Using appearance models and context based on room geometry. In *ECCV*. 2010. 1

[17] D. Hoiem, A. Efros, and M. Hebert. Putting objects in perspective. *CVPR*, 2006. 2

[18] D. Hoiem, A. A. Efros, and M. Hebert. Automatic photo pop-up. In *ACM Transactions on Graphics (TOG)*, 2005. 1

[19] D. Hoiem, A. A. Efros, and M. Hebert. Geometric context from a single image. *ICCV*, 2005. 1

[20] D. Hoiem, A. A. Efros, and M. Hebert. Closing the loop in scene interpretation. In *CVPR*, 2008. 1

[21] L. Kneip, D. Scaramuzza, and R. Siegwart. A novel parametrization of the perspective-three-point problem for a direct computation of absolute camera position and orientation. In *CVPR*, 2011. 3

[22] L. Ladickỳ, P. Sturgess, K. Alahari, C. Russell, and P. H. Torr. What, where and how many? combining object detectors and CRFs. In *ECCV*. 2010. 5

[23] Y. Li, N. Snavely, D. Huttenlocher, and P. Fua. Worldwide pose estimation using 3d point clouds. In *ECCV*. 2012. 1

[24] D. Lin, S. Fidler, and R. Urtasun. Holistic scene understanding for 3d object detection with rgbd cameras. In *ICCV*, 2013. 1

[25] M. Maire, S. X. Yu, and P. Perona. Hierarchical scene annotation. In *BMVC*, 2013. 6

[26] A. Martinović, M. Mathias, J. Weissenberg, and L. Van Gool. A three-layered approach to facade parsing. In *ECCV*. 2012. 5

[27] K. Matzen and N. Snavely. Nyc3dcars: A dataset of 3d vehicles in geographic context. In *ICCV*, 2013. 2, 3, 6, 7

[28] P. Moulon, P. Monasse, and R. Marlet. Adaptive structure from motion with a contrario model estimation. In *ACCV*. 2012. 3

[29] P. Moulon, P. Monasse, R. Marlet, and Others. Openmvg. an open multiple view geometry library. https://github.com/openMVG/openMVG. 3

[30] K. Murphy, A. Torralba, and W. Freeman. Using the forest to see the trees: a graphical model relating features, objects and scenes. *NIPS*, 2003. 1

[31] H. Riemenschneider, S. Sternig, M. Donoser, P. M. Roth, and H. Bischof. Hough regions for joining instance localization and segmentation. In *ECCV*. 2012. 5

[32] M. Rumpler, A. Irschara, A. Wendel, and H. Bischof. Rapid 3d city model approximation from publicly available geographic data sources and georeferenced aerial images. In *CVWW*, 2012. 2

[33] S. Satkin and M. Hebert. 3dnn: Viewpoint invariant 3d geometry matching for scene understanding. In *ICCV*, 2013. 1

[34] A. Saxena, M. Sun, and A. Y. Ng. Learning 3-d scene structure from a single still image. In *ICCV*, 2007. 1, 5, 6

[35] J. Shotton, J. Winn, C. Rother, and A. Criminisi. Textonboost: Joint appearance, shape and context modeling for multi-class object recognition and segmentation. In *ECCV*. 2006. 5

[36] N. Snavely, S. Seitz, and R. Szeliski. Modeling the world from internet photo collections. *IJCV*, 2007. 3

[37] M. Sun, S. Y. Bao, and S. Savarese. Object detection using geometrical context feedback. *IJCV*, 2012. 1

[38] H. Uchiyama, H. Saito, M. Servieres, and G. Moreau. AR GIS on a physical map based on map image retrieval using LLAH tracking. In *MVA*, 2009. 2

[39] L. Wang and U. Neumann. A robust approach for automatic registration of aerial images with untextured aerial lidar data. In *CVPR*, 2009. 2

[40] S. Wang, S. Fidler, and R. Urtasun. Holistic 3d scene understanding from a single geo-tagged image. 2015. 2, 8

[41] J. Xiao, J. Hays, K. A. Ehinger, A. Oliva, and A. Torralba. Sun database: Large-scale scene recognition from abbey to zoo. In *CVPR*, 2010. 7

[42] R. Yang and R. Yang. Action segmentation and recognition based on depth hog and probability distribution difference. In *ICIC*. 2014. 5